

Pharmacologic induction of innate immune signaling directly drives homologous recombination deficiency

Lena J. McLaughlin^{a,b,1}, Lora Stojanovic^{a,b,1}, Aksinija A. Kogan^{a,b}, Julia L. Rutherford^{a,b}, Eun Yong Choi^{b,c}, Ray-Whay Chiu Yen^d, Limin Xia^d, Ying Zou^{b,e}, Rena G. Lapidus^{b,c}, Stephen B. Baylin^{d,2}, Michael J. Topper^{d,2}, and Feyruz V. Rassool^{a,b,2}

^aDepartment of Radiation Oncology, University of Maryland School of Medicine, Baltimore, MD 21201; ^bProgram in Oncology, Marlene and Stewart Greenebaum Comprehensive Cancer Center, University of Maryland, Baltimore, MD 21201; ^cDepartment of Medicine, University of Maryland School of Medicine, Baltimore, MD 21201; ^dDepartment of Oncology, The Sidney Kimmel Comprehensive Cancer Center at Johns Hopkins, Baltimore, MD 21231; and ^eDepartment of Pathology, University of Maryland School of Medicine, Baltimore, MD 21201

Contributed by Stephen B. Baylin, May 26, 2020 (sent for review February 25, 2020; reviewed by Yang Shi and Weidong Wang)

Poly(ADP ribose) polymerase inhibitors (PARPi) have efficacy in triple negative breast (TNBC) and ovarian cancers (OCs) harboring BRCA mutations, generating homologous recombination deficiencies (HRDs). DNA methyltransferase inhibitors (DNMTi) increase PARP trapping and reprogram the DNA damage response to generate HRD, sensitizing BRCA-proficient cancers to PARPi. We now define the mechanisms through which HRD is induced in BRCA-proficient TNBC and OC. DNMTi in combination with PARPi up-regulate broad innate immune and inflammasome-like signaling events, driven in part by stimulator of interferon genes (STING), to unexpectedly directly generate HRD. This inverse relationship between inflammation and DNA repair is critical, not only for the induced phenotype, but also appears as a widespread occurrence in The Cancer Genome Atlas datasets and cancer subtypes. These discerned interactions between inflammation signaling and DNA repair mechanisms now elucidate how epigenetic therapy enhances PARPi efficacy in the setting of BRCA-proficient cancer. This paradigm will be tested in a phase I/II TNBC clinical trial.

homologous recombination deficiency | Fanconi anemia | stimulator of interferon signaling | poly(ADP-ribose) polymerase inhibitors | DNA methyltransferase inhibitors

Poly(ADP ribose) polymerase inhibitors (PARPi) are an exciting spectrum of antineoplastic drugs used in several major cancer types and are currently approved by the Food and Drug Administration (FDA) in ovarian cancers (OCs) and metastatic breast cancers (BCs) harboring germline BRCA mutations. PARP1 is an abundant nuclear protein that senses and contributes to repair of DNA single-strand breaks (SSBs) (1, 2), working through catalyzing poly-(ADP ribosyl)ation, or PARYlation, of itself, histones, and other target proteins (3). Blocking the catalytic activity of PARP1 has been shown to inhibit base excision repair (BER), resulting in accumulation of SSBs and generation of DNA double-strand breaks (DSBs), during replication (4), and this damage, in turn activates homologous recombination (HR) (5). The BRCA1 and BRCA2 proteins play critical roles in maintaining genomic stability through HR-mediated repair. PARPi prevents SSB repair, increasing DSBs, and ultimately leads to cell death through synthetic lethality. Although BRCA status has, to date, been the main factor predicting PARPi effectiveness, responses to PARPi therapy, even in BRCA-mutant cancers, have not been highly durable. Recent studies have shown that disruptions of any of several HR-related pathway events (6), including expression and/or function of Fanconi anemia (FA) (7) and *ATM* genes (8), can lead to HR deficiencies (HRDs) and, thus predict for sensitivity and tumor cytotoxicity to PARPi. Furthermore, PARPi have failed to show impressive clinical benefit for patients with sporadic estrogen-, progesterone- and her2-receptor negative, or triple negative breast cancers (TNBCs) (9), and/or other cancers with intact *BRCA* genes (BRCA-proficient). Thus,

there is a necessity for developing new strategies to maximize the efficacy of these agents and this is the focus of the present paper.

A key for the above need for improving PARPi therapy is the recent development of second-generation PARPi with much increased potency, such as talazoparib (Tal) (10). For this next generation of PARPi, their primary cytotoxic effects have been correlated with trapping of cytotoxic PARP1–DNA complexes at sites of SSBs and DSBs (8). Biochemically, such trapping at 5'-dRP lesions are generated during BER steps with PARPi treatment (8). This is well reflected in the fact that up to 100-fold greater inhibitory activity is associated with the increased ability of the potent PARPi, Tal, to trap PARP1–DNA complexes, compared to weaker PARPi such as veliparib (ABT888) (10).

In a recent study, our group has linked DNA methyltransferase inhibitors, (DNMTi) 5-azacytidine (Aza) and decitabine (Dac) to a potential strategy for improving the efficacy of Tal (11). DNMTi are approved by the FDA for treatment of myelodysplastic syndromes (MDSs) (12) and are also used for treatment of acute myeloid leukemia (AML) (13–15). These agents are potent inhibitors of DNMTs, thereby permitting reversion of DNA methylation through passive and active mechanisms (16). Reversing aberrant DNA methylation programs and the associated transcriptome in cancer is one proposed mechanism for the clinical efficacy of DNMTi (17, 18). During replication, DNMTi incorporate into DNA as an altered cytosine base and covalently bind DNMTs, creating a DNMT–DNA complex while simultaneously

Significance

Combining DNMTi with PARPi induces HRD in a BRCA-proficient setting. We now uncover an unexpected mechanism for generation of HRD that joins drug induction of a broad, innate immune signaling to directly drive HRD. The findings have important translational implications for broadening the scope of PARPi therapy and potentially for immunotherapy.

Author contributions: L.J.M., A.A.K., R.G.L., S.B.B., M.J.T., and F.V.R. designed research; L.J.M., L.S., J.L.R., E.Y.C., R.-W.C.Y., L.X., Y.Z., and M.J.T. performed research; L.J.M., L.S., Y.Z., R.G.L., and M.J.T. analyzed data; and L.J.M., S.B.B., M.J.T., and F.V.R. wrote the paper.

Reviewers: Y.S., Boston Children's Hospital; and W.W., NIH.

Competing interest statement: F.V.R. and S.B.B. are co-inventors on US Provisional Patent Application Number 61/929,680 for the concept of the combinatorial therapy.

Published under the [PNAS license](#).

Data deposition: Raw and processed data files related to gene expression microarray and RNA-seq datasets are available through the Gene Expression Omnibus (GEO) database repository under the accession IDs [GSE150298](#) and [GSE151317](#).

¹L.J.M. and L.S. contributed equally to this work.

²To whom correspondence may be addressed. Email: sbaylin@jhmi.edu, mtopper1@jhmi.edu, or frassool@som.umaryland.edu.

This article contains supporting information online at <https://www.pnas.org/lookup/suppl/doi:10.1073/pnas.2003499117/-DCSupplemental>.

First published July 10, 2020.

triggering the degradation of soluble DNMTs (19). In our above drug paradigm, low nanomolar doses of DNMTi in combination with the PARPi, Tal, leads to increased tight binding of DNMT1 and PARP1 in chromatin at SSBs, as well as at DSBs. These effects are dependent on interaction of both proteins, as depletion of each abolishes PARP1 localization to the above DNA damage sites (11). These dynamics produce synergistic cancer cell cytotoxicity and in vivo antitumor responses regardless of BRCA mutation status in TNBC and AML (11). Similar antitumor responses are also seen in BRCA-proficient OC with this drug combination (20).

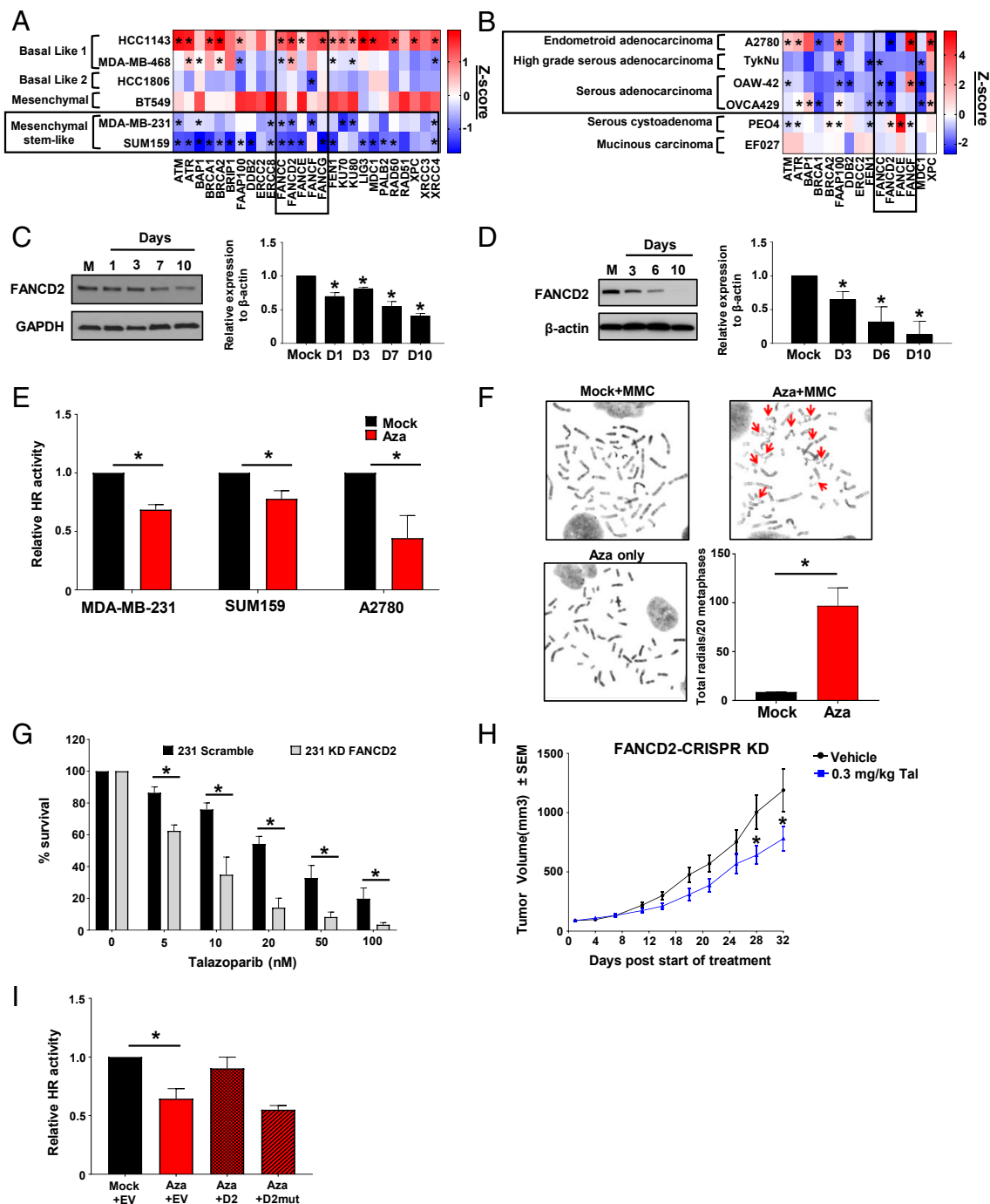
Low doses of DNMTi have been shown to reprogram the epigenome of multiple cancer pathways (16). We recently reported in lung cancer cells that DNMTi can induce HRD that sensitizes them to PARPi and radiation therapy (21). Another established action of DNMTi is to facilitate immune-related signaling across multiple cancer types (22, 23). We now, unexpectedly directly link these above immune actions of DNMTi, to the generation of HRD in TNBC and OC cells and hence sensitization to PARPi. The central coordinating mechanism for the above DNMTi immune signature has been centered on potentiation of interferon (IFN) α signaling induced by sensing of cytoplasmic double-stranded RNA (dsRNA), facilitated in part by the up-regulation of endogenous retroviral transcripts (ERVs) (24, 25). This phenomenon, termed DNMTi-induced viral mimicry (24, 25), enables the production of cytokines and attraction of activated CD8⁺ T lymphocytes to tumor sites, accompanied by antitumor responses (23, 26). In the current study, we broaden this DNMTi-induced potentiation of innate immune signaling to include not only cytosolic dsRNA, but also dsDNA with the latter being, in part, mediated by sensing through the reconstitution of stimulator of IFN genes (STING) signaling. Furthermore, these events are also associated with up-regulation of both nuclear factor kappa-light-chain enhancer of activated B cells (NF- κ B) and IFN α signaling. We suggest the term, pathogen mimicry response (PMR) to define this panoply of drug-induced signaling, which we link directly to down-regulation of FA genes to generate HRD, the emblematic molecular phenotype for fostering sensitivity to PARPi. Furthermore, we find that combining DNMTi with PARPi further augments immune-related signaling, potentiating HRD, or BRCAness phenotype in BRCA-proficient TNBC and OC cells. This mechanism suggests that DNMTi-PARPi therapy strategies can be deployed for the treatment of BRCA-proficient cancers, thus expanding the therapeutic utility of PARP inhibitors.

Results

Low Doses of DNMTi Generate an HRD Effect in BRCA-Proficient TNBC and OC. In a recent study, we have elucidated that in addition to the PARP1-DNA complexes in BRCA-proficient TNBC and AML, the combination of DNMTi plus PARPi also induce HRD in BRCA-proficient non-small cell lung cancer (NSCLC) (21). The mechanistic underpinnings of this DNMTi-induced HRD were not discerned, but the HRD involved down-regulation of FA genes, which play an important role in HR (21). Notably, we now observe similar DNMTi-induced dynamics occurring in BRCA-proficient TNBC and OC. Thus, in the TNBC cell lines MDA-MB-231 and SUM159PT, treatment with low doses of the DNMTi Aza (500 nM and 250 nM Aza, respectively) induces down-regulation of BRCAness genes (boxed area, Fig. 1A and *SI Appendix, Fig. S1A*), including several FA-related genes and critically FANCD2, which is central to the interaction between FA and HR and the progression to HR-mediated repair (27). Intriguingly, these cell lines have mesenchymal stem-like features (28), as opposed to other subtypes that did not show the same expression pattern (Fig. 1A). Likewise, several BRCA-proficient OC cells, including A2780, OAW-42, and OVCA429, demonstrated decreases in expression of multiple BRCAness genes, again, including FANCD2 following low-dose Aza (150 to 500 nM) treatment (boxed area, Fig. 1B and *SI Appendix, Fig. S1B*). These above decreases in gene expression

following Aza treatment result in a parallel decrease in steady-state levels of FANCD2 protein in both BRCA-proficient TNBCs (MDA-MB-231) (Fig. 1C) and OC cells (A2780) (Fig. 1D) and are associated with a functional decrease in HR activity, as monitored by a GFP reporter assay (direct repeat [DR]-GFP) (Fig. 1E and *SI Appendix, Fig. S1C*) (29). As a further validation of this HRD effect in BRCA-proficient cell lines, MDA-MB-231 TNBC and A2780 OC cells, Aza (150 to 500 nM) decreases levels of Rad51 foci (30) (*SI Appendix, Fig. S1D and E*) after induction of DSBs with ionizing (IR) (4 Gy) treatment, as measured by γ H2AX (*SI Appendix, Fig. S1F and G*). As expected, Rad51 recruitment is not impaired after induction of IR damage in the Aza-treated TNBC cell line HCC1143 where Aza induces an up-regulation of BRCAness-related genes (Fig. 1A and *SI Appendix, Fig. S1H*). Finally, decreases in FANCD2 have a classic phenotypic consequence, increased triradial chromosomes in cells treated with the DNA cross-linking drug, mitomycin C (MMC) (31). This is not observed in MDA-MB-231 TNBCs (Fig. 1F) and A2780 OC (*SI Appendix, Fig. S1I*) cells treated with Aza or MMC alone, but the increase of chromosomal abnormalities and radial chromosome formations is apparent when the drugs are combined. Transient knockdown of FANCD2 to similar levels induced by low-dose DNMTi treatment in MDA-MB-231 (*SI Appendix, Fig. S1J*) reduced HR activity to levels comparable with the drug-induced response (*SI Appendix, Fig. S1K*). This link between down-regulation of FANCD2 to a drug-induced HRD phenotype matches with the predicted increased sensitivity to Tal in clonogenic assays using stable knockdown of this protein compared to scrambled controls (Fig. 1G and *SI Appendix, Fig. S1L–N*). These results are not restricted to in vitro studies, as MDA-MB-231 cells with comparable levels of FANCD2-CRISPR-KD have significant growth inhibition when implanted as xenografts in immunodeficient mice treated with Tal (Fig. 1H and *SI Appendix, Fig. S1O and P*). Importantly in these studies, Aza effects on HR activity in MDA-MB-231 can be partially rescued by overexpression of constructs for wild type, but not catalytically dead mutant FANCD2 or empty vector controls (Fig. 1I).

DNMTi and PARPi Induce Global Perturbation of the Transcriptome Providing a Link between DNA Repair and Innate Immune Signaling Pathways. Several previous studies have linked DNMTi treatment to global alteration of the transcriptome, inclusive of innate immune-related signatures in tumor cells (22, 23) and a notably similar signature also occurs with PARPi treatment (32, 33). In agreement, TNBC and OC cells, display transcriptome-wide alteration with the generation of many differentially expressed genes (DEGs), resulting from the administration of the pharmacologic agents under study (*SI Appendix, Fig. S2 A–C*). Among these DEGs, are those related to the perturbation of DNA repair, as detailed in the previous section, including distinct subsets of genes showing differential sensitivity to each therapy (*SI Appendix, Fig. S2 D and E*). Further evaluation of DNA repair genes specifically revealed, in agreement with qRT-PCR expression analyses after Aza treatment (Fig. 1A and B and *SI Appendix, Fig. S1A and B*), the down-regulation of several BRCAness genes contained within the Fanconi anemia pathway including: BRIP1, FANCC, FANCD2, and FANCF (*SI Appendix, Fig. S2 D and E*). Regarding FANCD2 specifically, which was the focus of the preceding section, Aza treatment imparts significant repression in both MDA-MB-231 (Fig. 2A) and A2780 (*SI Appendix, Fig. S2F*), with additional down-regulation noted from combination treatment in MDA-MB-231 (Fig. 2A). Importantly, the perturbations noted above for DNA repair genes, occurs in the absence of substantive alteration of cell cycle distribution (*SI Appendix, Fig. S2G*). To elucidate whether more general pathway level changes are facilitated by the pharmacologic agents under investigation, we utilized standard gene set enrichment analysis (GSEA) (34), with specific querying of the



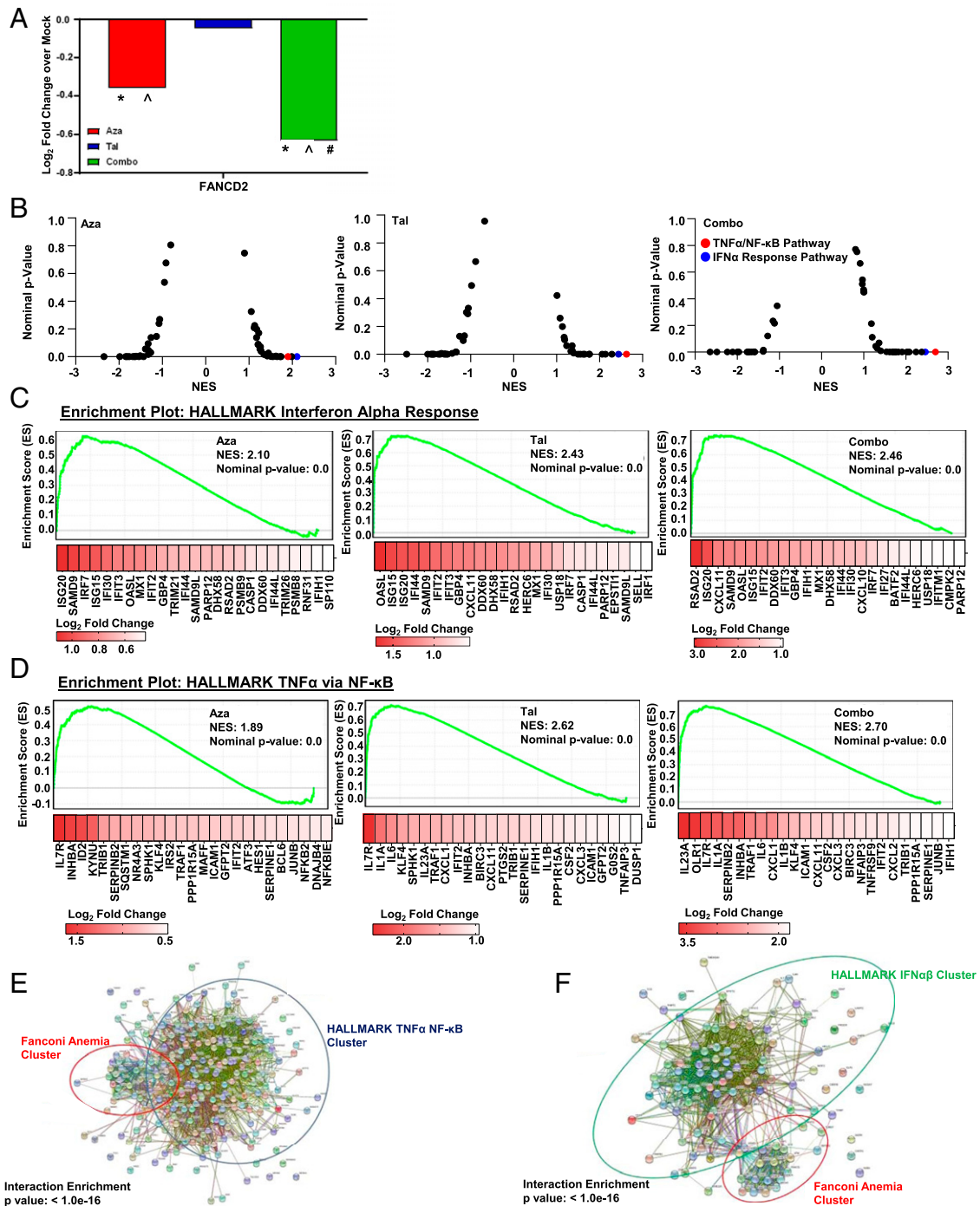


Fig. 2. DNMTi and PARPi induce global perturbation of transcriptome providing a link between DNA repair and innate immune signaling pathways. (A) FANCD2 expression change in RNA-seq dataset for MDA-MB-231 day 10, y axis: Log₂ fold change relative to mock, significance obtained by DESeq2 pairwise comparison: * $P < 0.05$ vs. mock, $\Delta P < 0.05$ vs. Tal, $\#P < 0.05$ vs. Aza (500 nM Aza, 10 nM Tal, Combo: 500 nM Aza + 10 nM Tal; mock $n = 4$, Aza $n = 4$, Combo $n = 3$). (B) HALLMARK gene set normalized enrichment score (NES) volcano plot for MDA-MB-231 day 10 total transcriptome RNA-seq data DESeq2 analysis: (Left) 500 nM Aza, (Center) 10 nM Tal, (Right) Combo: 500 nM Aza + 10 nM Tal; x axis: NES, y axis: nominal P value. Each dot is a single HALLMARK pathway (50 total), red dots: TNF α /NF- κ B gene set, blue dot: IFN α gene set, black dot: other pathway. (C) NES plots for MDA-MB-231 day 10 total transcriptome RNA-seq data HALLMARK IFN α response. For each plot: y axis: enrichment score (degree of overrepresentation of detected genes in ranked dataset), x axis: ranked gene list. Below each plot: heatmap based on Log₂ fold change (color gradation white to red, low to high) detected for top 25 genes of leading-edge subset for each. NES plots are ordered as follows: (Left) 500 nM Aza, (Center) 10 nM Tal, (Right) Combo: 500 nM Aza + 10 nM Tal. (D) NES plots for MDA-MB-231 day 10 total transcriptome RNA-seq data HALLMARK TNF α via NF- κ B. For each plot: y axis: enrichment score, x axis: ranked gene list. Below each plot: heatmap based on Log₂ fold change (color gradation white to red, low to high) detected for top 25 genes of leading-edge subset for each. NES plots are ordered as follows: (Left) 500 nM Aza, (Center) 10 nM Tal, (Right) Combo: 500 nM Aza + 10 nM Tal. (E) STRING protein-protein interaction map of Fanconi anemia pathway vs. TNF α /NF- κ B pathway-related genes. Gene sets depicted derived from MSigDB (Broad Institute). See [SI Appendix, Fig. S2K](#) for an expanded version. (F) STRING protein-protein interaction map of Fanconi anemia pathway vs. IFN α pathway-related genes. Gene sets depicted derived from MSigDB (Broad Institute). See [SI Appendix, Fig. S2L](#) for an expanded version.

HALLMARK gene set (35). This approach allows for evaluation of coordinated changes in gene expression linked to specific biological processes. These analyses revealed a preponderance of immune-related gene sets present in top positively enriched pathways, with further enhancement noted in drug combination-treated samples versus monotherapies alone (Fig. 2B and *SI Appendix, Fig. S2H*). This immune gene set enrichment revealed an expanded scope for both DNMTi and PARPi transcriptional augmentation, and in addition to up-regulation of cytosolic dsRNA sensing, which leads to IFN $\alpha\beta$ induction, the data now reveal signaling for tumor necrosis factor α (TNF α)/NF- κ B with IFN $\alpha\beta$ gene sets as top “hits” across our datasets (Fig. 2B and *SI Appendix, Fig. S2H* and Table S1). One notable exception to the aforementioned generalized trend, is the down-regulation of IFN $\alpha\beta$ pathway genes by the application of Tal in A2780 cells, occurring in concert with the induction of TNF α /NF- κ B-related genes (*SI Appendix, Fig. S2H*). These data highlight that while both gene sets are innate immune related, transcriptional alteration may not be a synchronous event. Although these innate immune pathways were enriched significantly by both DNMTi and PARPi, the highest induction was facilitated by combination treatment in terms of both overall pathway normalized enrichment score (NES) and leading-edge gene augmentation (Fig. 2C and D and *SI Appendix, Fig. S2I* and J). Regarding the significance of NES and leading-edge gene-based readouts, NES is the primary statistic derived from GSEA and provides a metric for statistically significant concordant changes in a specific pathway, for which leading edge genes contribute most to noted pathway enrichment.

Importantly, we establish the convergence of these above drug-induced transcriptional responses, namely immune-related signaling and BRCAness through querying of STRING (search tool for the retrieval of interacting genes/proteins). STRING is a compiled database that allows for the identification of both known interactions and strength of evidence for connections between targets of interest (36). These data reveal a highly significant interaction, and hence a potential basal relationship, between FA pathway members and IFN $\alpha\beta$ or TNF α /NF- κ B-related genes (Fig. 2E and F, and *SI Appendix, Fig. S2K* and L). Thus, in total, the above data reveal a pharmacologic response centered on the perturbation of immune-related datasets occurring in concert with the repression of DNA repair gene subsets, and furthermore, these datasets reveal a direct functional association in the basal state.

A Basal, Inverse Correlation Exists between Pathogen Response Pathways and FA-Related Gene Sets. The above connectivity maps demonstrate an interaction between immune-related and FA group genes, but these data alone, do not reveal whether there is an inverse relationship as predicted by our drug studies. This inverse relationship emerges from evaluation of The Cancer Genome Atlas (TCGA) (37) and Molecular Taxonomy of Breast Cancer International Consortium (METABRIC) (38) expression data sets deposited in the cBioPortal (39, 40). Analyses of these mRNA data reveals an overall negative correlation, by Pearson correlation, between BRCAness genes and IFN $\alpha\beta$ or TNF α /NF- κ B genes in both TNBC and OC datasets (Fig. 3A and *SI Appendix, Table S2*). Furthermore, this inverse relationship appears across several major cancer types, including, pancreatic ductal adenocarcinoma, colon adenocarcinoma, lung adenocarcinoma, lung squamous cell carcinoma, and AML datasets (*SI Appendix, Fig. S3A* and B).

Finally, based on our pharmacologic transcriptional data as detailed in the preceding sections, we selected FANCD2, FANCC, and FANCE for further evaluation. In agreement with the global pattern discerned across the entire dataset, FANCD2, FANCC, and FANCE display a conserved overall negative correlation, most pronounced when compared with TNF α /NF- κ B pathway-associated genes (Fig. 3B and C). Expanding these gene-specific analyses to

other BRCAness genes reveals, in agreement with the above correlation plots, the existence of a broad inverse, basal transcriptional program in both TNBC and OC. Intriguingly, OC demonstrates a more pronounced negative correlation between IFN $\alpha\beta$ genes and BRCAness genes when compared with TNBC (*SI Appendix, Fig. S3C–F*). These TCGA and METABRIC data when considered in the aggregate reveal a basal, inverse transcriptional correlation between BRCAness genes and innate immune genes conserved across major human cancer types.

Acute TNF α and IFN β Cytokine Treatment Down-Regulates BRCAness Genes and Induces HRD. To functionally follow the above-suggested correlations, we next sought to define whether a causal relationship exists between inflammatory/IFN signaling and DNA repair and related genes. The application of exogenous TNF α in TNBC and OC reveals a seminal role for this signaling in the creation of HRD. TNF α is known to initiate inflammatory signaling processes (41, 42) through the potentiation of NF- κ B signaling by facilitating the proteasomal degradation of I κ B and nuclear translocation of NF- κ B homo- or heterodimers (43, 44). As further evidence of NF- κ B causation, we evaluated HRD in the presence of exogenous cytokine stimulation. Indeed, the application of TNF α induced a marked increase in expression of TNF α /NF- κ B responsive genes, as expected, with a correlated repression of several BRCAness genes in TNBC cells, and notably, FANCC and UBE2T in OC cell lines (Fig. 4A and B). Accompanying these gene responses was an associated repression of functional HR activity in both TNBC and OC cells (Fig. 4C and D). Additionally, the application of IFN β in both TNBC and OC, as expected, induces a marked increase in expression of IFN-sensitive genes (ISGs), with a correlated repression of several BRCAness genes (Fig. 4E and F), all of which occur in the absence of appreciable alteration of cell cycle distribution (*SI Appendix, Fig. S4A*). Accompanying these gene expression responses was an associated significant functional HR defect in both MDA-MB-231 and A2780 cells but this effect was most pronounced in the TNBC system (Fig. 4G and H). Importantly, simultaneous treatment with the Jak 1/2 inhibitor, ruxolitinib, (45), which blocks downstream STAT signaling and ISG stimulation (46), fully rescues the HR activity defect imparted by exogenous IFN β (Fig. 4G and H). Consistent with the above IFN signaling-mediated HRD, similar results were obtained by treatment of TNBC and OC cells with Poly I:C, a cytosolic dsRNA mimetic and potent inducer of IFN signaling (47, 48) (Fig. 4G and H and *SI Appendix, Fig. S4B* and C). The application of the dsDNA mimetic Poly dI:dC resulted in a more measured response relative to IFN β and Poly I:C in both TNBC and OC (Fig. 4G and H and *SI Appendix, Fig. S4D* and E). Interestingly, MDA-MB-231 TNBC cells were found to be far more sensitive to poly I:C relative to poly dI:dC, while A2780 cells demonstrated less basal sensitivity to either of these mimetics despite a noted HRD response (Fig. 4G and H), thus suggesting that cytosolic nucleotides represent only part of the repair gene down-regulation mechanism. These data provide direct evidence that IFN β and TNF α /NF- κ B-related signaling can induce BRCAness and provides validation for the proposed inverse relationship between expression of IFN stimulated genes or TNF α /NF- κ B-related genes and BRCAness genes as displayed in both pan-cancer TCGA/METABRIC and our pharmacologic transcriptional data. These data also reveal that repression of DNA repair genes by perturbation of this innate immune signaling, inclusive of both IFN $\alpha\beta$ and TNF α /NF- κ B-related signaling, may have phenotypic implications in the facilitation of PARPi sensitization for BRCA-proficient TNBC and OC.

DNMTi and PARPi Induce Chronic Inflammatory and IFN $\alpha\beta$ -Related Signaling. A conserved feature of the IFN $\alpha\beta$ transcriptional response, which has emerged in previous studies induced by both

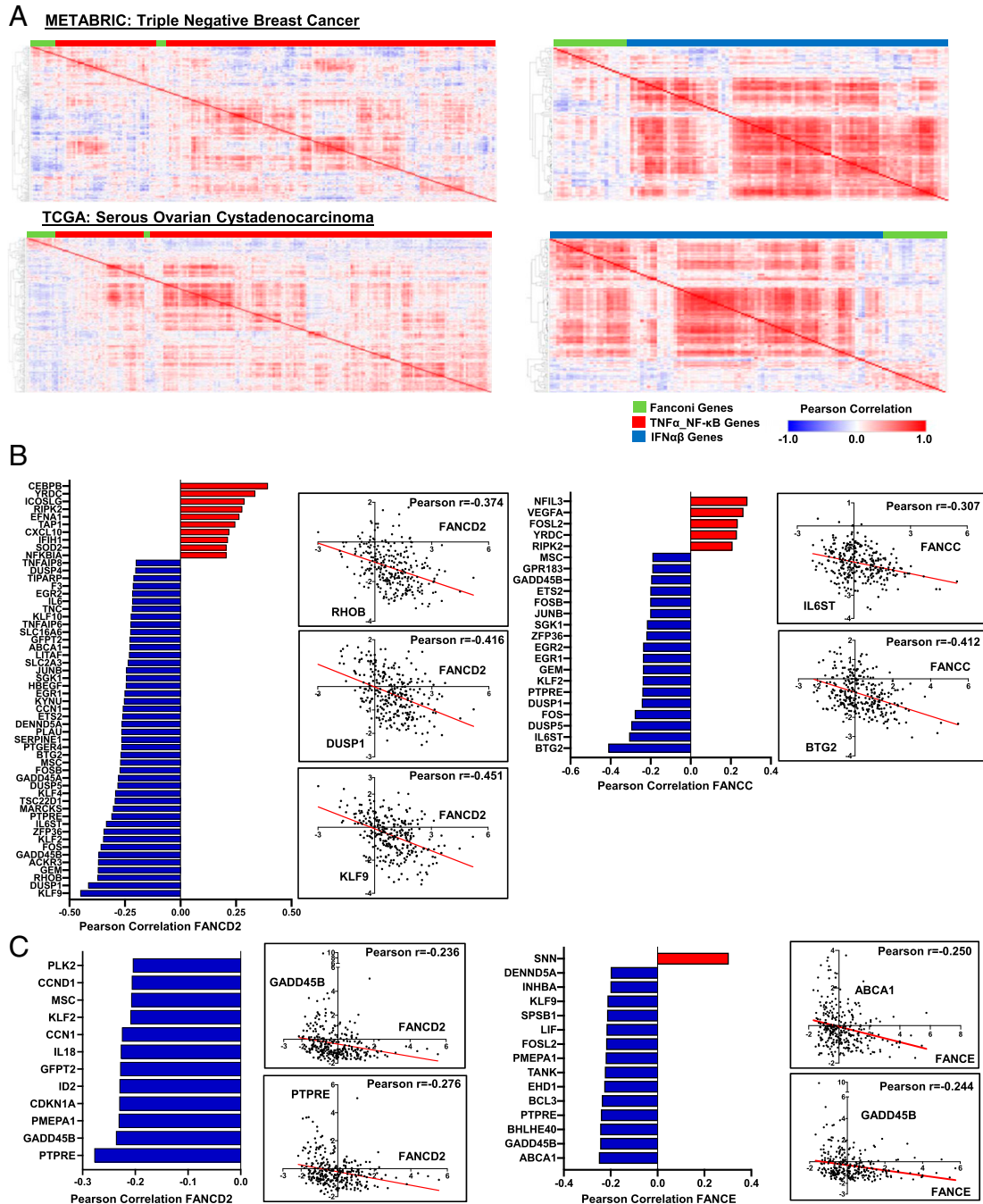


Fig. 3. Basal, inverse correlation exists between pathogen response pathways and FA- related gene sets. (A, Top) Pearson correlation-based heatmaps for METABRIC TNBC samples (mRNA expression [microarray] Z scores). Clustering by one minus Pearson correlation, negative correlation, blue; positive correlation, red. (Left) Fanconi anemia pathway-related genes (green bar) vs. TNF α /NF- κ B pathway-related genes (red bar). (Right) Fanconi anemia pathway-related genes (green bar) vs. IFN α β pathway-related genes (blue bar). (A, Bottom) Pearson correlation-based heatmaps for TCGA serous ovarian cystadenocarcinoma (mRNA expression Z scores, RSEM [batch normalized]). Clustering by one minus Pearson correlation, negative correlation, blue; positive correlation, red. (Left) Fanconi anemia pathway-related genes (green bar) vs. TNF α /NF- κ B pathway-related genes (red bar). (Right) Fanconi anemia pathway-related genes (green bar) vs. IFN α β pathway-related genes (blue bar). (B) Bar plots of Pearson correlation coefficients for METABRIC TNBC samples (mRNA expression [microarray] Z scores). Genes selected based on absolute value greater than 0.20 and significant P value after multiple comparisons correction (FDR set at 0.01 to define P value threshold for discovery). Blue bar = negative correlation, red bar = positive correlation with FANCD2 (Left) or FANCC (Right). Representative scatterplots (x and y axes are the Z scores for genes contained, where each dot is representative of a single patient in dataset) are depicted immediately right of each bar plot. (C) Bar plots of Pearson correlation coefficients for TCGA serous ovarian cystadenocarcinoma (mRNA expression Z scores, RSEM [batch normalized]). Genes selected based on absolute value greater than 0.20 and significant P value after multiple comparisons correction (FDR set at 0.01 to define P value threshold for discovery). Blue bar = negative correlation, red bar = positive correlation with FANCD2 (Left) or FANCE (Right). Representative scatterplots (x and y axes are the Z scores for genes contained, where each dot is representative of a single patient in dataset) are depicted immediately right of each bar plot.

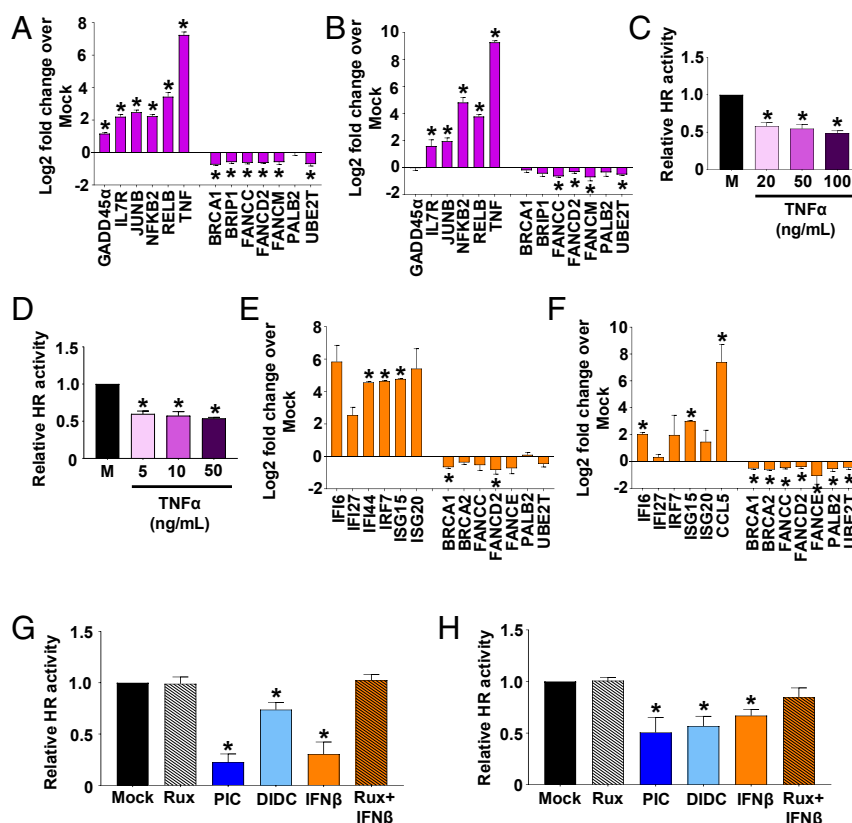


Fig. 4. Acute TNF α and IFN β cytokine treatment down-regulates BRCAness genes and induces HRD. (A and B) Relative RNA expression for a subset of TNF α inflammatory and FA/HR genes after stimulation with 8 to 12 h and 5 to 100 ng/mL TNF α in MDA-MB-231 (A) and A2780 (B). (qRT-PCR, $n = 3$). (C and D) Relative HR activity analysis of GFP $^{+}$ cells by flow cytometry 72 h after transient transfection of I-SceI for 6 h, followed by 5 to 100 ng/mL TNF α treatment in MDA-MB-231:DR-GFP (C) and A2780:DR-GFP (D) cell lines ($n = 3$). (E and F) Relative RNA expression for a subset of IFN β pathway and FA/HR genes after stimulation with 8 to 12 h and 100 ng/mL IFN β in MDA-MB-231 (E) and A2780 (F). (qRT-PCR, $n = 3$). (G and H) Relative HR activity analysis of GFP $^{+}$ cells by flow cytometry 72 h after 6 h transient transfection of I-SceI followed by 5 μ M ruxolitinib, 100 ng/mL IFN β , or 5 μ M ruxolitinib + 100 ng/mL IFN β , or after 6 h transient transfection of I-SceI + 0.5 to 1 mg/mL Poly(I:C) or I-SceI + 0.5 to 1 mg/mL Poly(dI:dC) in MDA-MB-231:DR-GFP (G) and A2780:DR-GFP (H) cell lines ($n = 3$). All data are presented as mean \pm SEM with statistical significance derived from two-tailed unpaired Student's t test (or ANOVA). *Adjusted P value <0.05 after (FDR = 0.05) based multiple comparisons correction, two-stage linear step-up procedure of Benjamini, Kriegerm, and Yekutieli.

DNMTi (22, 23, 25, 26, 49) and PARPi treatment (32, 50), is downstream IFN gene stimulation, and we now link this further to include TNF α /NF- κ B inflammatory signaling. Evaluation of qRT-PCR data for drug-induced changes in TNF α /NF- κ B-related genes, revealed a generalized transcriptional increase present after a 72-h treatment and persisting through day 6 and day 10 in both TNBC and OC (Fig. 5 A and B and *SI Appendix, Fig. S5 A and B*). In this regard, TNF α /NF- κ B-related gene augmentation as a result of our pharmacologic treatments was more pronounced in the DNMTi + PARPi combination relative to single agent alone, and more apparent in TNBC relative to OC. Evaluation of canonical IFN α -related genes by qRT-PCR, reveals a similar temporal pattern as discerned for TNF α /NF- κ B-related genes, with transcriptional augmentation initiating at 72 h after treatment in both MDA-MB-231 and A2780 cells and persisting until day 10 (Fig. 5 C and D and *SI Appendix, Fig. S5 C and D*). Indeed, several IFN α -related genes contained in this panel that show induction with Aza or Tal, are further increased in combination-treated cells across cell lines, including CCL5, IFI27, IRF7, and ISG20 for TNBC (Fig. 5C and *SI Appendix, Fig. S5C*). In contrast, IFN α gene augmentation is entirely Aza driven with significant induction of CCL5, IFI27, and TMEM173 noted in OC (Fig. 5D and *SI Appendix, Fig. S5D*).

The above-detailed transcriptional responses were preceded, as expected by nuclear translocation of both p65/p50 in both MDA-MB-231 and A2780 occurring predominantly in an Aza-

driven manner, with further augmentation noted by combination treatment (Fig. 5 E and F). p50 and p65 are the predominant subunits responsible for NF- κ B-mediated gene activation and bind to target genes as p50/p65 or p50/p50, hetero- and homodimers, respectively (51, 52). As further validation of the hypothesis that inflammation and associated genes might perturb the expression of DNA repair genes, we evaluated two additional TNBC cell lines (MDA-MB-468 and HCC1806) that do not induce BRCAness in response to Aza, as shown in Fig. 1A. These data demonstrate that relative to MDA-MB-231, these “non-responder” cell lines fail to notably down-regulate DNA repair genes or induce IFN α and TNF α /NF- κ B-related genes from Aza treatment (*SI Appendix, Fig. S5E*). As expected, transient knockdown with siRNAs targeting NF- κ B and dsDNA-sensing pathway genes induces augmentation of FANCD2 expression in both mock- and Aza-treated MDA-MB-231 TNBC cells compared to nontargeting controls (*SI Appendix, Fig. S5 F and G*). These data in total are suggestive of a sustained increase in inflammatory signaling and related genes as the result of our therapeutic combination and that this innate immune signaling might be sufficient to induce BRCAness.

STING Pathway Augmentation Facilitates HRD through Transcriptional Repression of FANCD2. Further interrogation of inflammatory signaling uncovers an additional parameter, which acts to facilitate

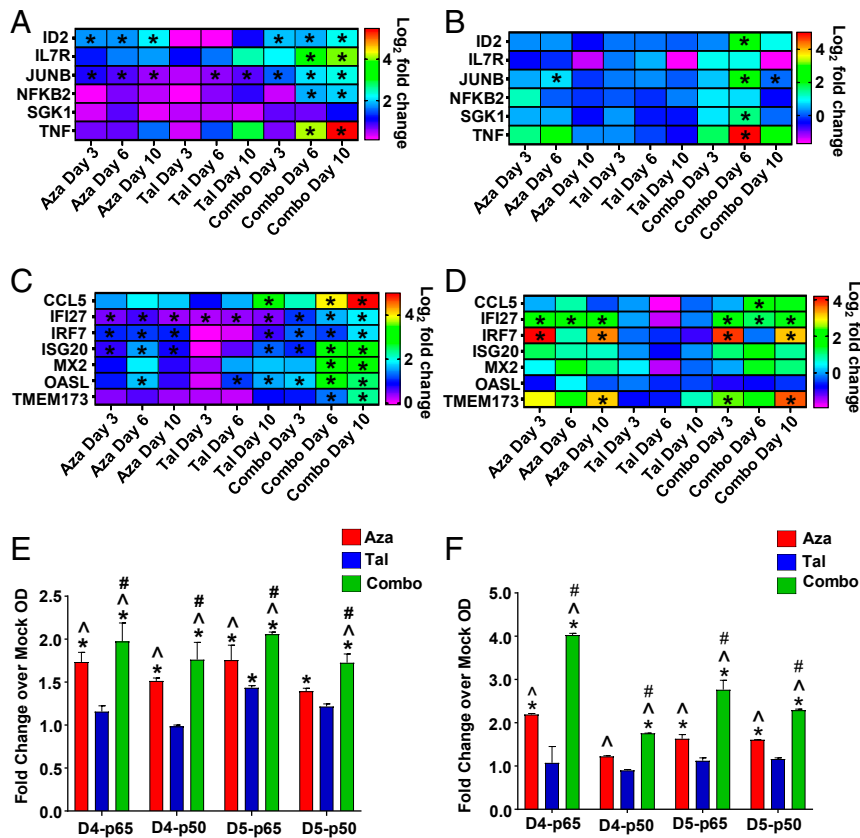


Fig. 5. DNMTi and PARPi induces chronic inflammatory and IFN α -related signaling. (A and B) Log₂-based heatmaps depicting relative RNA expression over time for a subset of TNF α inflammatory pathway genes in MDA-MB-231 (A) treated with vehicle, 500 nM Aza, 10 nM Tal, or Combo: 500 nM Aza + 10 nM Tal, and A2780 (B) treated with vehicle, 150 nM Aza, 2.5 nM Tal, or Combo: 150 nM Aza + 2.5 nM Tal. (qRT-PCR, day 3, day 6, and day 10, $n = 3$). (C and D) Log₂-based heatmaps depicting relative RNA expression over time for a subset of IFN β pathway genes in MDA-MB-231 (C) treated with vehicle, 500 nM Aza, 10 nM Tal, or Combo: 500 nM Aza + 10 nM Tal, and A2780 (D) treated with vehicle, 150 nM Aza, 2.5 nM Tal, or Combo: 150 nM Aza + 2.5 nM Tal. (qRT-PCR, day 3, day 6, and day 10, $n = 3$). (E) TransAM NF- κ B activation (p50/p65) colorimetric ELISA for MDA-MB-231 day 4 (D4) and day 5 (D5) nuclear extracts (10 μ g per condition) treated as follows: 500 nM Aza, 10 nM Tal, or Combo: 500 nM Aza + 10 nM Tal. x axis, treatment and time point; y axis, fold change over mock optical density (OD) 450 nm. ($n = 2$). (F) TransAM NF- κ B activation (p50/p65) colorimetric ELISA for A2780 D4 and D5 nuclear extracts (10 μ g per condition) treated as follows: 150 nM Aza, 2.5 nM Tal, or Combo: 150 nM Aza + 2.5 nM Tal. x axis, treatment and time point; y axis, fold change over mock OD 450 nm. ($n = 2$) All data are presented as mean \pm SEM with statistical significance derived from two-tailed unpaired Student's t test or ANOVA * vs. mock, ^ vs. Tal, # vs. Aza for adjusted P value <0.05 after (FDR = 0.05) based on multiple comparisons correction, two-stage linear step-up procedure of Benjamini, Kriegerm, and Yekutieli.

the described PMR and associated HRD. This signaling involves a critical pathway node responsive to cytosolic dsDNA, which can be triggered by DNA viruses and bacterial infections, namely stimulator of IFN signaling, or STING (53). The first suggestions of this resulted from Kyoto Encyclopedia of Genes and Genomes (KEGG) pathway analyses of transcriptional data (54), which reveal sensing of cytosolic DNA as a top pathway enriched by either monotherapy and especially their combination (Fig. 6A and *SI Appendix*, Fig. S64). In concert with this enhanced transcriptional response, increases in cytosolic DNA are observed across all conditions assayed, with the most pronounced induction by Tal- and drug combination-treated samples (Fig. 6B). Focusing on STING specifically, we observe that STING mRNA is increased across all drug conditions, with further augmentation noted in drug combination-treated samples (*SI Appendix*, Fig. S64). Intriguingly, increases in STING protein are driven solely by Aza treatment and not observed with Tal treatment alone, but there is further accumulation noted in drug combination-treated samples (Fig. 6C). These alterations in STING protein occur in the absence of detectable changes in other pathway components, cGAS or TBK1, both of which are required for canonical STING signaling (Fig. 6C). In addition to the above transcriptional and

protein perturbations of STING signaling, we uncover a central role for STING in the facilitation of HRD and transcriptional BRCAness. Drug treatment in the presence of STING inhibition, results in reversion of HRD in both Aza and combination-treated samples, attaining statistical significance in the Aza-treated group (Fig. 6D). Additionally, we find that the application of siRNA-mediated depletion of STING (*SI Appendix*, Fig. S6B) or STING-specific inhibition, are able to rescue the Aza-induced repression of FANCD2, while only the former is able to fully rescue combination FANCD2 repression (Fig. 6E and *SI Appendix*, Fig. S6C). In contrast, STING overexpression alone in the absence of other stimuli, such as DNA damage, has no effect on FANCD2 expression (*SI Appendix*, Fig. S6D). Furthermore, the knockdown of STING by siRNA markedly dampens the induction of inflammation-associated gene expression (Fig. 6F and *SI Appendix*, Fig. S6E). These STING-associated data suggest that Aza and combination-induced repair gene repression with associated HRD is at least partially dependent on the presence of competent STING signaling. Furthermore, STING signaling appears critical for the facilitation of the inflammation-associated gene induction imparted by our pharmacologic paradigm.

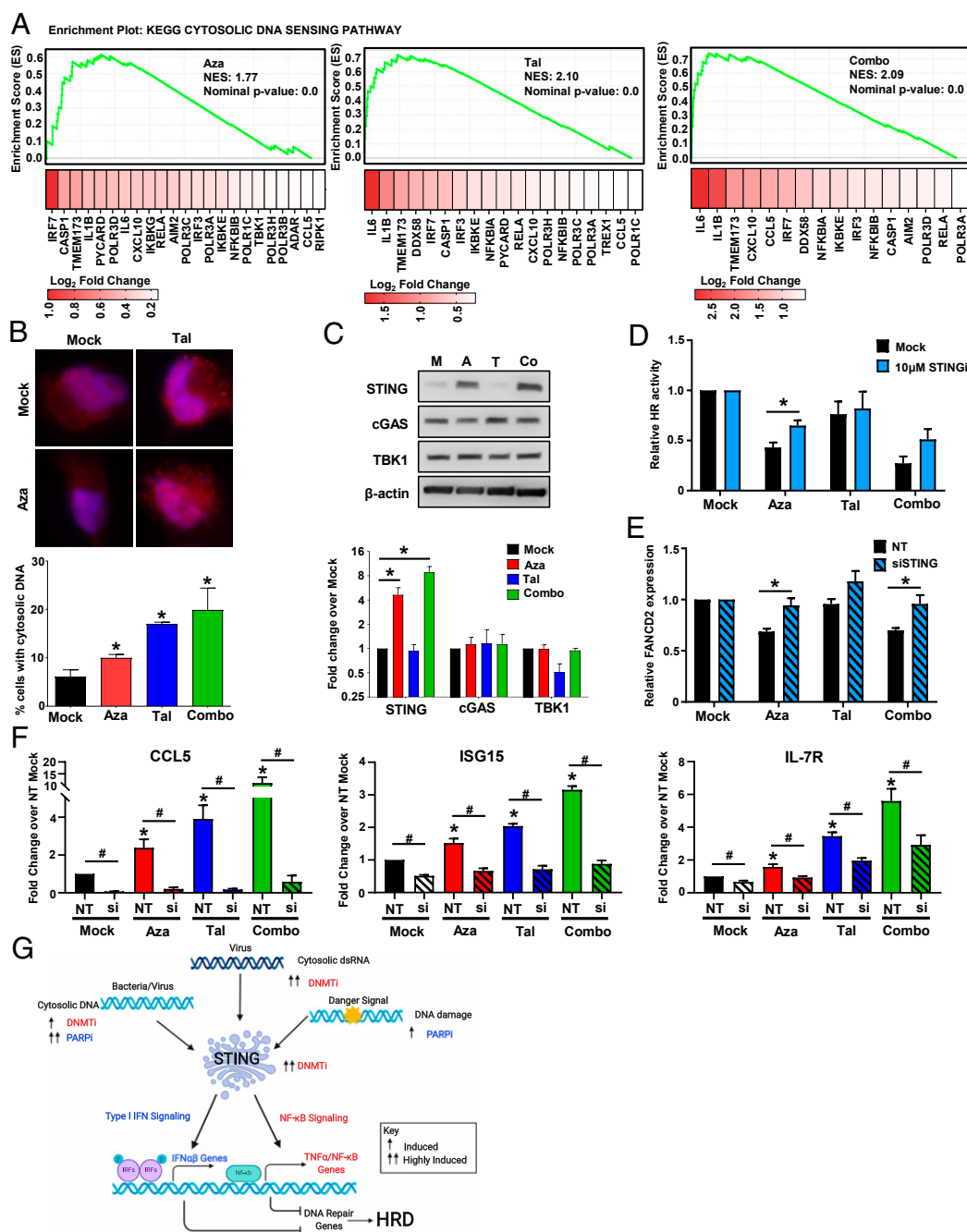


Fig. 6. STING pathway augmentation by DNMTi and PARPi facilitates HRD through transcriptional repression of FANCD2. (A) KEGG cytosolic DNA-sensing pathway NES plots for MDA-MB-231 day 10 total transcriptome RNA-seq data. For each plot: y axis, enrichment score; x axis, compiled ranked genes. Below each plot: heatmap based on Log₂ fold change (color gradation white to red) detected for leading edge gene subset in each panel. NES plots are ordered: (Left) 500 nM Aza, (Middle) 10 nM Tal, (Right) Combo: 500 nM Aza + 10 nM Tal. (B) Representative immunofluorescence images for dsDNA (Top) and quantified (Bottom) in MDA-MB-231 after vehicle, 500 nM Aza, 10 nM Tal, or Combo: 500 nM Aza + 10 nM Tal treatment (day 6, *n* = 3). (C) Immunoblot for STING, cGAS, and TBK1 in MDA-MB-231 treated with vehicle (M), 500 nM Aza (A), 10 nM Tal (T), or Combo: 500 nM Aza + 10 nM Tal (Co) with β-actin used as a loading control (Top) and quantified (Bottom) (day 6, *n* = 3). (D) Relative HR activity analysis of GFP⁺ cells by flow cytometry after 6-h transient transfection of I-SceI in 231:DR-GFP after 6-d treatment with vehicle, 500 nM Aza, 10 nM Tal, or Combo: 500 nM Aza + 10 nM Tal, ±10 μM STINGi for all conditions (*n* = 3). (E) Relative FANCD2 expression after transient knockdown using siSTING for 24 h followed by 6 d treatment of vehicle, 500 nM Aza, 10 nM Tal, or Combo: 500 nM Aza + 10 nM Tal (qRT-PCR, day 6, *n* = 3). (F) Relative CCL5 (Left), ISG15 (Middle), and IL-7R (Right) expression after transient knockdown using nontarget controls (NT) or siSTING (si) for 24 h followed by treatment of vehicle, 500 nM Aza, 10 nM Tal, or Combo: 500 nM Aza + 10 nM Tal (qRT-PCR, day 6, *n* = 3). (G) Schematic of a multifaceted inflammatory response, which leads to HRD in TNBC and OC. In the proposed model for the combination therapy, the DNMTi induction of viral mimicry via cytosolic dsRNA combined with the PARPi increase of cytosolic dsDNA, converge to the activation of a DNMTi reconstituted STING signaling pathway. This activated response leads to a transcriptional increase in IFNα/β and TNFα/NF-κB signaling, which facilitates the transcriptional repression of FA/HR DNA repair-associated genes in a STING-dependent manner. The overall drug-induced pathogen mimicry response creates a BRCAness phenotype and thus enhances sensitivity to PARPi in the BRCA-proficient setting. All data are presented as mean ± SEM with statistical significance derived from two-tailed unpaired Student's *t* test (or ANOVA). * vs. mock and # as indicated for adjusted *P* value <0.05 after (FDR = 0.05) based on multiple comparisons correction, two-stage linear step-up procedure of Benjamini, Krieger, and Yekutieli.

While the role of STING in cytosolic DNA detection is well described (53, 55, 56), the implications of this signaling node extends beyond this single parameter to include dsRNA detection and DNA damage response (32, 57, 58). Our above experimental findings are most consistent with the multifaceted nature of STING acting to integrate distinct signaling outcomes depending on the context of activation. Importantly, recent reports demonstrate that STING signals downstream predominantly through IRF- or NF- κ B-dependent mechanisms, depending greatly on stimulation type (57). The latter of these two pathways seems more in line with pharmacologically induced signaling detected in TNBC and OC cells (Fig. 5 A–D). In summary, Aza and Aza/Tal drug combination treatment up-regulates PMR, dependent on the presence of intact STING signaling, and the activation of this inflammatory response facilitates a BRCAness phenotype and PARPi sensitization (Fig. 6G).

Discussion

The results presented herein support an expanded view of DNMTi-induced activation of innate immune signaling, encompassing not only viral mimicry via the cytoplasmic dsRNA-sensing system, but also in the broader context of mimicking a complex cellular PMR. Moreover, DNMTi and the DNMTi/PARPi drug combination induce a confluence of signaling events, leading to IFN α β and TNF α /NF- κ B signaling, partially dependent on intact STING signaling. Joining these above events, across both TNBC and OC, there is a direct link to the above immune-related signaling and BRCAness, or HRD phenotype, which is the sine qua non for sensitizing tumor cells to the DNA damage effects of PARPi.

The role of STING signaling in our present observations is particularly intriguing and merits special comments. Several other studies have linked STING activation to the actions of PARPi (33, 50, 59) and our present study expands this understanding to a mechanistic context for the regulation of BRCAness gene expression in BRCA-proficient settings. The seminal finding is the involvement of STING in a multifaceted PMR, wherein each pharmacologic component provides critical aspects to potentiate related signaling. The resulting inflammatory signaling mediates the facilitation of HRD through transcriptional decreases in BRCAness genes. This noted BRCAness might act to enhance the same signaling mechanism, wherein the accumulation of damage might act to potentiate the PMR response detailed above and may underlie the enhanced response observed in drug combination-treated samples.

There are several additional implications of our present findings from both a basic and translational perspective. First, it is interesting to speculate about the evolutionary aspects of our now identified connection between inflammation and the facilitation of HRD by transcriptional repression of BRCAness genes. The induction of HRD could operate within the context of the cellular death response inherent to inflammasome signaling and its role for cellular pathogen responses. This complex signaling process has evolved to provide a robust mechanism to trigger death when virally or bacterially infected cells cannot clear the pathogen (60, 61). Extrapolating this to tumorigenesis, the leading risk for cancer is the presence of chronic inflammation, and renewing cells must learn to bypass this cell death response to participate in the early steps to tumorigenesis. Such a scenario might then be characteristic of cell populations at risk for epigenetic and genetic abnormalities, which can contribute to cancer initiation and progression and may be reversible by epigenetic therapies (62, 63). Reestablishing inflammatory signaling and resultant HRD might then be a potent approach to sensitizing such cancer cells to killing effects. Such a role may also be played by STING agonists (64, 65) and their use in the clinic will be followed with interest.

The above dynamics can be extrapolated to an ultimate translational potential, extending the use of PARPi in cancer therapy by using these drugs in combination with epigenetic therapy to activate innate immune pathways and to subsequently create HRD. We have previously shown that combining DNMTi and PARPi in vitro and in vivo, triggers cytotoxic tumor cell DNA damage and death with a noted increase in overall survival of treated mice implanted with wild-type, BRCA-proficient human AML and breast cancer cell lines (11). A clinical trial of AML based on these previous findings is ongoing for DNMTi plus Tal. Our current insight achieved in the present study now provides even more compelling evidence for why the combination of a DNMTi plus a PARPi might be an efficacious therapy approach in solid cancers. As we have noted earlier, at present, a critical driver of PARPi efficacy is the presence of BRCAness and HRD (66). However, this scenario is largely restricted to patients with BC and OC whose tumors harbor mutations in *BRCA* genes and treatment of such patients is currently the only FDA approval scenario for use of PARPi (66, 67). Our newly described connection between activating inflammasome-linked signaling and inducing potent BRCAness and HRD is occurring in TNBC and OC cells which are wild type for *BRCA* genes. Hence, our findings have great potential relevance for a treatment approach that could widely expand the use of PARPi in important cancer treatment scenarios for these as well as other cancer types, including NSCLC. Indeed, we have recently seen the creation of HRD in lung cancer cells treated with DNMTi plus PARPi prior to our recognizing the present link to inflammasome-related signaling (21). The results in the current study now serve as the underpinning for a now-enrolling clinical trial using a DNMTi plus the PARPi, Tal, in patients with BC whose tumors harbor wild-type *BRCA* genes. Importantly, the immune signaling events and creation of HRD we now have elucidated may provide substrate for correlative science studies in this trial. We can now query a wide range of immune and HR biomarkers in pre- vs. posttreatment tumor biopsies to develop signatures, which will help predict and monitor efficacy of our combination therapy approach.

Materials and Methods

See *SI Appendix, Materials and Methods* for a detailed description of cell lines, drug reagents, and treatments in vitro and in vivo, lentiviral transductions, colony-forming assay, irradiation, analysis of chromosomal breaks, RNA interference, RNA extraction, qRT-PCR, microarray sample isolation and labeling, microarray hybridization and data extraction, primers, protein extraction and immunoblotting, antibodies, immunofluorescence staining, HR repair analysis, nuclear lysate-based ELISA, siRNA screen, STING vector-based overexpression, microarray gene expression analysis, GSEA, RNA sequence (RNA-seq) library preparation and analysis, TCGA and METABRIC Pearson correlation analysis, STRING protein–protein interaction map, TCGA and METABRIC correlation bar plots, and statistical analysis.

Data Availability. Raw and processed data files related to gene expression microarray and RNA-seq datasets are available through the Gene Expression Omnibus (GEO) database repository under the accession ID GSE150298 and GSE151317.

ACKNOWLEDGMENTS. Our studies have been supported by funding from the Van Andel Institute–Stand up to Cancer (S.B.B. and F.V.R.); the Adelson Medical Research Foundation (L.J.M., L.S., J.L.R., M.J.T., F.V.R., and S.B.B.); Evelyn Grollman Glick Scholar (M.J.T.); The Hodson Trust (M.J.T.); the Leukemia Lymphoma Society (A.A.K. and F.V.R.); the Maryland Department of Health's Cigarette Restitution Fund Program (F.V.R.); the National Cancer Institute–Cancer Center Support Grant P30 CA134274 University of Maryland Marlene and Stewart Greenebaum Comprehensive Cancer Center (R.G.L., E.Y.C., and F.V.R.); the Molecular Medicine Graduate Program, University of Maryland (L.J.M. and A.A.K.); the Biochemistry Graduate Program, University of Maryland (J.L.R.); and the Human Genetics Graduate Program, University of Maryland (L.S.). R.-W.C.Y. is supported by the Commonwealth Foundation and the Defense Health Program, through the Department of Defense Ovarian Cancer Research Program, Teal Innovator Award OC130454/W81XWH-14-1-0385. Opinions, interpretations, conclusions, and recommendations are those of the authors and not necessarily endorsed by the Department of Defense.

1. M. De Vos, V. Schreiber, F. Dantzer, The diverse roles and clinical relevance of PARPs in DNA damage repair: Current state of the art. *Biochem. Pharmacol.* **84**, 137–146 (2012).
2. M. Audebert, B. Salles, P. Calsou, Involvement of poly(ADP-ribose) polymerase-1 and XRCC1/DNA ligase III in an alternative route for DNA double-strand breaks rejoining. *J. Biol. Chem.* **279**, 55117–55126 (2004).
3. B. A. Gibson, W. L. Kraus, New insights into the molecular and cellular functions of poly(ADP-ribose) and PARPs. *Nat. Rev. Mol. Cell Biol.* **13**, 411–424 (2012).
4. G. Mariano *et al.*, PARP inhibitor ABT-888 affects response of MDA-MB-231 cells to doxorubicin treatment, targeting Snail expression. *Oncotarget* **6**, 15008–15021 (2015).
5. M. Chevanne *et al.*, Inhibition of PARP activity by PJ-34 leads to growth impairment and cell death associated with aberrant mitotic pattern and nucleolar actin accumulation in M14 melanoma cell line. *J. Cell. Physiol.* **222**, 401–410 (2010).
6. J. Mateo *et al.*, DNA-repair defects and olaparib in metastatic prostate cancer. *N. Engl. J. Med.* **373**, 1697–1708 (2015).
7. A. D. D'Andrea, Susceptibility pathways in Fanconi's anemia and breast cancer. *N. Engl. J. Med.* **362**, 1909–1919 (2010).
8. J. Murai *et al.*, Trapping of PARP1 and PARP2 by clinical PARP inhibitors. *Cancer Res.* **72**, 5588–5599 (2012).
9. M. Guha, PARP inhibitors stumble in breast cancer. *Nat. Biotechnol.* **29**, 373–374 (2011).
10. Y. Shen, M. Aoyagi-Scharber, B. Wang, Trapping poly(ADP-ribose) polymerase. *J. Pharmacol. Exp. Ther.* **353**, 446–457 (2015).
11. N. E. Muvarak *et al.*, Enhancing the cytotoxic effects of PARP inhibitors with DNA demethylating agents—A potential therapy for cancer. *Cancer Cell* **30**, 637–650 (2016).
12. H. Kantarjian *et al.*, Decitabine improves patient outcomes in myelodysplastic syndromes: Results of a phase III randomized study. *Cancer* **106**, 1794–1803 (2006).
13. M. Carbone *et al.*, PARP-1 interaction with VP1 capsid protein regulates polyomavirus early gene expression. *J. Mol. Biol.* **363**, 773–785 (2006).
14. M. Zampieri *et al.*, ADP-ribose polymers localized on Ctcf-Parp1-Dnmt1 complex prevent methylation of Ctcf target sites. *Biochem. J.* **441**, 645–652 (2012).
15. J. P. Issa *et al.*, Phase 1 study of low-dose prolonged exposure schedules of the hypomethylating agent 5-aza-2'-deoxycytidine (decitabine) in hematopoietic malignancies. *Blood* **103**, 1635–1640 (2004).
16. H. C. Tsai *et al.*, Transient low doses of DNA-demethylating agents exert durable anti-tumor effects on hematological and epithelial tumor cells. *Cancer Cell* **21**, 430–446 (2012).
17. J. P. Issa, DNA methylation as a therapeutic target in cancer. *Clin. Cancer Res.* **13**, 1634–1637 (2007).
18. S. B. Baylin, P. A. Jones, A decade of exploring the cancer epigenome—Biological and translational implications. *Nat. Rev. Cancer* **11**, 726–734 (2011).
19. K. Patel *et al.*, Targeting of 5-aza-2'-deoxycytidine residues by chromatin-associated DNMT1 induces proteasomal degradation of the free enzyme. *Nucleic Acids Res.* **38**, 4313–4324 (2010).
20. N. Pulliam *et al.*, An effective epigenetic-PARP inhibitor combination therapy for breast and ovarian cancers independent of BRCA mutations. *Clin. Cancer Res.* **24**, 3163–3175 (2018).
21. R. Abbotts *et al.*, DNA methyltransferase inhibitors induce a BRCAness phenotype that sensitizes NSCLC to PARP inhibitor and ionizing radiation. *Proc. Natl. Acad. Sci. U.S.A.* **116**, 22609–22618 (2019).
22. J. Wrangle *et al.*, Alterations of immune response of non-small cell lung cancer with azacytidine. *Oncotarget* **4**, 2067–2079 (2013).
23. M. J. Topper *et al.*, Epigenetic therapy ties MYC depletion to reversing immune evasion and treating lung cancer. *Cell* **171**, 1284–1300.e21 (2017).
24. K. B. Chiappinelli *et al.*, Inhibiting DNA methylation causes an interferon response in cancer via dsRNA including endogenous retroviruses. *Cell* **162**, 974–986 (2015).
25. D. Roulois *et al.*, DNA-demethylating agents target colorectal cancer cells by inducing viral mimicry by endogenous transcripts. *Cell* **162**, 961–973 (2015).
26. M. L. Stone *et al.*, Epigenetic therapy activates type I interferon signaling in murine ovarian cancer to reduce immunosuppression and tumor burden. *Proc. Natl. Acad. Sci. U.S.A.* **114**, E10981–E10990 (2017).
27. H. Kim, A. D. D'Andrea, Regulation of DNA cross-link repair by the Fanconi anemia/BRCA pathway. *Genes Dev.* **26**, 1393–1408 (2012).
28. B. D. Lehmann *et al.*, Identification of human triple-negative breast cancer subtypes and preclinical models for selection of targeted therapies. *J. Clin. Invest.* **121**, 2750–2767 (2011).
29. N. Bannardo, A. Cheng, N. Huang, J. M. Stark, Alternative-NHEJ is a mechanistically distinct pathway of mammalian chromosome break repair. *PLoS Genet.* **4**, e1000110 (2008).
30. M. Graeser *et al.*, A marker of homologous recombination predicts pathologic complete response to neoadjuvant chemotherapy in primary breast cancer. *Clin. Cancer Res.* **16**, 6159–6168 (2010).
31. L. H. Thompson, J. M. Hinz, Cellular and molecular consequences of defective Fanconi anemia proteins in replication-coupled DNA repair: Mechanistic insights. *Mutat. Res.* **668**, 54–72 (2009).
32. J. Shen *et al.*, PARPi triggers the STING-dependent immune response and enhances the therapeutic efficacy of immune checkpoint blockade independent of BRCAness. *Cancer Res.* **79**, 311–319 (2019).
33. R. M. Chabanon *et al.*, PARP inhibition enhances tumor cell-intrinsic immunity in ERCC1-deficient non-small cell lung cancer. *J. Clin. Invest.* **129**, 1211–1228 (2019).
34. A. Subramanian *et al.*, Gene set enrichment analysis: A knowledge-based approach for interpreting genome-wide expression profiles. *Proc. Natl. Acad. Sci. U.S.A.* **102**, 15545–15550 (2005).
35. A. Liberzon *et al.*, The Molecular Signatures Database, The Molecular Signatures Database (MSigDB) hallmark gene set collection. *Cell Syst.* **1**, 417–425 (2015).
36. C. von Mering *et al.*, STRING: Known and predicted protein-protein associations, integrated and transferred across organisms. *Nucleic Acids Res.* **33**, D433–D437 (2005).
37. J. N. Weinstein *et al.*, Cancer Genome Atlas Research Network, The Cancer Genome Atlas Pan-Cancer analysis project. *Nat. Genet.* **45**, 1113–1120 (2013).
38. C. Curtis *et al.*, METABRIC Group, The genomic and transcriptomic architecture of 2,000 breast tumours reveals novel subgroups. *Nature* **486**, 346–352 (2012).
39. E. Cerami *et al.*, The cBio cancer genomics portal: An open platform for exploring multidimensional cancer genomics data. *Cancer Discov.* **2**, 401–404 (2012).
40. J. Gao *et al.*, Integrative analysis of complex cancer genomics and clinical profiles using the cBioPortal. *Sci. Signal.* **6**, pii (2013).
41. G. D. Kalliolias, L. B. Ivashkiv, TNF biology, pathogenic mechanisms and emerging therapeutic strategies. *Nat. Rev. Rheumatol.* **12**, 49–62 (2016).
42. F. Balkwill, TNF-alpha in promotion and progression of cancer. *Cancer Metastasis Rev.* **25**, 409–416 (2006).
43. E. J. Duh, W. J. Maury, T. M. Folks, A. S. Fauci, A. B. Rabson, Tumor necrosis factor alpha activates human immunodeficiency virus type 1 through induction of nuclear factor binding to the NF-kappa B sites in the long terminal repeat. *Proc. Natl. Acad. Sci. U.S.A.* **86**, 5974–5978 (1989).
44. J. W. Lowenthal, D. W. Ballard, E. Böhlein, W. C. Greene, Tumor necrosis factor alpha induces proteins that bind specifically to kappa B-like enhancer elements and regulate interleukin 2 receptor alpha-chain gene expression in primary human T lymphocytes. *Proc. Natl. Acad. Sci. U.S.A.* **86**, 2331–2335 (1989).
45. C. Harrison, A. M. Vannuchi, Ruxolitinib: A potent and selective Janus kinase 1 and 2 inhibitor in patients with myelofibrosis. An update for clinicians. *Ther. Adv. Hematol.* **3**, 341–354 (2012).
46. W. M. Schneider, M. D. Chevillotte, C. M. Rice, Interferon-stimulated genes: A complex web of host defenses. *Annu. Rev. Immunol.* **32**, 513–545 (2014).
47. H. F. Lindh, H. L. Lindsay, B. R. Mayberry, M. Forbes, Polyinosinic-cytidylic acid complex (poly I:C) and viral infections in mice. *Proc. Soc. Exp. Biol. Med.* **132**, 83–87 (1969).
48. A. A. Tytell, G. P. Lampson, A. K. Field, M. M. Nemes, M. R. Hilleman, Influence of size of individual homopolynucleotides on the physical and biological properties of complexed rIn:Cn (poly I:C). *Proc. Soc. Exp. Biol. Med.* **135**, 917–921 (1970).
49. H. Li *et al.*, Immune regulation by low doses of the DNA methyltransferase inhibitor 5-azacitidine in common human epithelial cancers. *Oncotarget* **5**, 587–598 (2014).
50. C. Pantelidou *et al.*, PARP inhibitor efficacy depends on CD8⁺ T-cell recruitment via intratumoral STING pathway activation in BRCA-deficient models of triple-negative breast cancer. *Cancer Discov.* **9**, 722–737 (2019).
51. A. Oeckinghaus, S. Ghosh, The NF-kappaB family of transcription factors and its regulation. *Cold Spring Harb. Perspect. Biol.* **1**, a000034 (2009).
52. T. Huxford, G. Ghosh, A structural guide to proteins of the NF-kappaB signaling module. *Cold Spring Harb. Perspect. Biol.* **1**, a000075 (2009).
53. H. Ishikawa, Z. Ma, G. N. Barber, STING regulates intracellular DNA-mediated, type I interferon-dependent innate immunity. *Nature* **461**, 788–792 (2009).
54. M. Kanehisa, S. Goto, KEGG: Kyoto encyclopedia of genes and genomes. *Nucleic Acids Res.* **28**, 27–30 (2000).
55. X. Cai, Y. H. Chiu, Z. J. Chen, The cGAS-cGAMP-STING pathway of cytosolic DNA sensing and signaling. *Mol. Cell* **54**, 289–296 (2014).
56. H. Ishikawa, G. N. Barber, STING is an endoplasmic reticulum adaptor that facilitates innate immune signalling. *Nature* **455**, 674–678 (2008).
57. G. Dunphy *et al.*, Non-canonical activation of the DNA sensing adaptor STING by ATM and IFI16 mediates NF-kappaB signaling after nuclear DNA damage. *Mol. Cell* **71**, 745–760.e5 (2018).
58. K. M. Franz, W. J. Neidermyer, Y. J. Tan, S. P. J. Whelan, J. C. Kagan, STING-dependent translation inhibition restricts RNA virus replication. *Proc. Natl. Acad. Sci. U.S.A.* **115**, E2058–E2067 (2018).
59. R. M. Chabanon, J. C. Soria, C. J. Lord, S. Postel-Vinay, Beyond DNA repair: The novel immunological potential of PARP inhibitors. *Mol. Cell. Oncol.* **6**, 1585170 (2019).
60. S. L. Fink, B. T. Cookson, Apoptosis, pyroptosis, and necrosis: Mechanistic description of dead and dying eukaryotic cells. *Infect. Immun.* **73**, 1907–1916 (2005).
61. H. Ashida *et al.*, Cell death and infection: A double-edged sword for host and pathogen survival. *J. Cell Biol.* **195**, 931–942 (2011).
62. Y. Tao *et al.*, Aging-like spontaneous epigenetic silencing facilitates Wnt activation, stemness, and Braf(V600E)-induced tumorigenesis. *Cancer Cell* **35**, 315–328.e6 (2019).
63. L. Xia *et al.*, CHD4 has oncogenic functions in initiating and maintaining epigenetic suppression of multiple tumor suppressor genes. *Cancer Cell* **31**, 653–668.e7 (2017).
64. J. M. Ramanjulu *et al.*, Design of amidobenzimidazole STING receptor agonists with systemic activity. *Nature* **564**, 439–443 (2018).
65. S. M. McWhirter *et al.*, A host type I interferon response is induced by cytosolic sensing of the bacterial second messenger cyclic-di-GMP. *J. Exp. Med.* **206**, 1899–1911 (2009).
66. C. J. Lord, A. Ashworth, PARP inhibitors: Synthetic lethality in the clinic. *Science* **355**, 1152–1158 (2017).
67. C. J. Lord, A. N. Tutt, A. Ashworth, Synthetic lethality and cancer therapy: Lessons learned from the development of PARP inhibitors. *Annu. Rev. Med.* **66**, 455–470 (2015).